ILETA International Information and Engineering Technology Association

International Journal of Heat and Technology

Vol. 43, No. 1, February, 2025, pp. 251-260

Journal homepage: http://iieta.org/journals/ijht

Thermodynamic-Based Rock Temperature Response and Geological Structure Evolution Simulation



Sicheng Lu¹, Shuqiang Lu², Yunjing Cui², Yi Song³, Bin Wang⁴, Rui Fu^{3*}, Zeyu Wang³

- ¹ National Field Observation and Research Station of Landslides in Three Gorges Reservoir Area of Yangtze River, China Three Gorges University, Yichang 443002, China
- ² Key Laboratory of Geological Hazards on Three Gorges Reservoir Area, Ministry of Education, China Three Gorges University, Yichang 443002, China
- ³ Jilin Province Water Resource and Hydropower Consultative Company of P. R. China, Changchun 130026, China
- ⁴ The Fourth Geological Exploration Institute Co., Ltd of Henan, Zhengzhou 450001, China

Corresponding Author Email: ruifu13@163.com

Copyright: ©2025 The authors. This article is published by IIETA and is licensed under the CC BY 4.0 license (http://creativecommons.org/licenses/by/4.0/).

https://doi.org/10.18280/ijht.430126

Received: 12 August 2024 Revised: 17 December 2024 Accepted: 25 December 2024 Available online: 28 February 2025

Keywords:

rock temperature response, geological structure evolution, moving grid method, heat source temperature inversion, geothermal gradient

ABSTRACT

The rock temperature response is closely related to geological structure evolution and is a crucial tool for studying Earth's internal dynamics, geothermal distribution, and structural evolution. The temperature distribution of rocks is influenced not only by the geothermal gradient but also by factors such as tectonic activity and heat source distribution. Currently, predicting rock temperature responses and simulating geological structure evolution have become significant topics in the field of geology. However, existing studies often rely on simplified heat conduction equations or empirical models, neglecting the complexity of geological structures and the uneven distribution of heat sources. This results in limited prediction accuracy and efficiency in large-scale areas or complex geological contexts. Moreover, traditional temperature inversion methods fail to fully consider the heterogeneity between tectonic units, limiting their application effectiveness in geological structure evolution simulations. To address these issues, this paper proposes a thermodynamic-based method for simulating rock temperature responses and geological structure evolution. The main content of the study includes two aspects: first, rock temperature response prediction based on the moving grid method, which efficiently handles temperature field distribution under complex geological structures; second, rock temperature inversion for geological structure evolution simulation, providing a more precise method for simulating geological structure evolution. Through this research, the paper aims to improve the accuracy and efficiency of rock temperature response prediction and provide a new theoretical framework and technical means for understanding subsurface thermodynamic processes and geological structure evolution.

1. INTRODUCTION

With the continuous advancement of geological research, the relationship between rock temperature response and geological structure evolution has received increasing attention. The temperature distribution of rocks is not only closely related to the geothermal gradient but also influenced by factors such as crustal movement, heat flow, and the physical properties of rocks [1-4]. The prediction and simulation of rock temperature response have become an important topic in geological research for the analysis of tectonic movements, magmatic activities, and sedimentary processes. Through an in-depth study of rock temperature response, we can not only deepen our understanding of geological structure evolution but also provide theoretical support for resource exploration and geological disaster early warning.

The study of rock temperature response and geological structure evolution has significant scientific meaning and

practical value. Changes in the temperature field of rocks can reflect the distribution and activity of heat sources in the crust, revealing the dynamic processes in the deep underground, especially in the study of tectonic belts, volcanic belts, and regions with heat flow anomalies [5, 6]. Accurate prediction of the rock temperature field can better understand the interaction between tectonic changes and thermodynamic processes, providing a reliable theoretical basis for geological disaster prediction, resource exploration, and energy development [7-13]. More importantly, the study of rock temperature response provides an important research window for revealing the evolution of deep underground materials, the relationship between thermodynamic and mechanical processes, and the long-term dynamics of crustal evolution.

Although some research has explored the relationship between rock temperature response and geological structure evolution, existing methods still have certain limitations. Most existing temperature prediction models rely on simple heat conduction equations or empirical formulas, neglecting the uneven distribution of actual geological structures and heat sources. Some studies use numerical simulation methods, which can simulate the temperature distribution in local areas well, but there are still significant gaps in computational accuracy and efficiency when handling large-scale regions and complex geological structures [14-17]. Furthermore, current research often lacks effective methods for heat source temperature inversion, which limits the accuracy and reliability of geological structure evolution simulations. For example, traditional temperature inversion methods fail to fully consider the complex thermal response of different tectonic units, leading to large deviations in inversion results, which cannot accurately predict the temperature evolution process of different geological historical stages [18-21].

This paper aims to propose a new thermodynamic-based method for simulating rock temperature response and geological structure evolution. The main research content includes two parts: First, the rock temperature response prediction based on the moving grid method, which can efficiently and accurately handle the temperature field distribution under complex geological structures and uneven heat source conditions; second, the rock temperature inversion for geological structure evolution simulation, which simulates the evolution process of geological structures by inverting the heat source temperature and provides a more accurate basis for temperature field prediction. Through these two studies, this paper can not only improve existing rock temperature response prediction methods but also provide more reliable theoretical tools and technical means for the dynamic simulation of geological structure evolution, thus offering new perspectives and approaches to better understand underground thermodynamic processes, geological structures, and their evolution patterns.

2. ROCK TEMPERATURE RESPONSE PREDICTION BASED ON THE MOVING GRID METHOD

Figure 1 shows the principle of rock temperature response under the influence of the surface heat flow field. Surface heat flow is not only affected by the geothermal gradient but is also closely related to underground heat source activities and crustal structural changes. In traditional static grid methods, since the computational grid remains unchanged between different time steps, the complex variations in the surface heat flow field during the geological structure evolution process are often overlooked. In practical applications, especially when influenced by solar radiation or crustal movement, the computational grid tends to change. For example, the movement of the solar radiation center can lead to grid updates, causing the grids at different times to be inconsistent. In the Mckenzie model, if the computational grids at two time steps are different, the heat flow information generated at the previous time step may not be accurately recognized by the new grid at the subsequent time step, which in turn affects the accuracy of temperature response prediction. Therefore, using the moving grid method can dynamically update the computational grid and capture changes in the surface heat flow in real-time, providing more accurate and timely heat flow data for subsequent temperature response predictions.

By continuously updating the grid positions and distribution according to the changes in geological structure, it ensures that each computational grid is adapted to the current geological background. This dynamic grid can flexibly respond to surface heat flow fluctuations caused by geological activities, capturing the processes of heat flow propagation, energy generation, and dissipation in a timely manner. It is especially capable of reflecting changes in heat sources and how heat propagates in different directions, particularly in complex tectonic belts and volcanic activity regions. When the grid is updated, the heat flow information from the previous time step may not be directly compatible with the new grid, so it is necessary to transfer and adjust the heat flow data based on the relationship between the two grids. This process involves topological analysis of grids from different time steps, and through interpolation, the heat flow data from the previous time step is adapted to the current grid to ensure the continuity and accuracy of the temperature response.

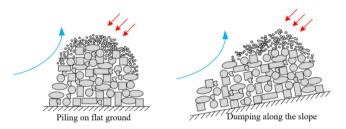


Figure 1. Principle of rock temperature response under the influence of surface heat flow field

To achieve real-time monitoring of surface heat flow propagation and energy generation and dissipation processes, this paper combines the Mckenzie model with a spectral interpolation numerical method to ensure the accurate transfer and update of surface heat flow information between different time steps, thus providing effective support for real-time monitoring of rock temperature response. In the Mckenzie model, the surface heat flow field is described by the twodimensional distribution of the spectral density $V(\delta, \phi)$. This spectral density not only describes the energy distribution of surface heat flow at different frequencies and directions but also reflects the impact of dynamic geological structure changes on heat flow propagation. Therefore, accurately updating the spectral energy density information generated at the previous time step to the new grid nodes at the next time step is crucial to ensuring the accuracy of real-time monitoring.

In the specific numerical method, the spectral density data of the first set of grid nodes at time S needs to be determined. For each grid node, the distribution of the spectral density at different frequencies and directions has already been effectively described in the calculation results at time S. Then, at time S+1, by comparing the new grid node positions with the geographical locations of the grid nodes at time S, we can select the two nearest grid nodes. The spectral density data of these two grid nodes will be used to estimate the spectral density of the new grid node. Specifically, the average frequency and direction angle of the two selected grid nodes can help calculate the spectral density of the new node. Assuming the grid node is numbered by u and the spectral frequency time step is represented by u, the average frequency of these points can be obtained by the following formula:

$$l_{u,j} = \int V_u(\delta, \phi) \delta^j f \delta f \phi \tag{1}$$

To calculate the spectral density of the new node, the average frequency of these two grid nodes must first be obtained. This is done by weighted averaging the frequencies

of the two nodes, with the weights typically determined by the distance relationship between the nodes. With the calculated average frequency and direction angle, the spectral density of the new grid node can be determined. Specifically, the average frequency of node *i* can be obtained by the following formula:

$$\overline{\delta}_{u} = \frac{l_{u,s+1}}{l_{u,s}} \tag{1}$$

Assuming that the geographical distance from node 1 to the grid point is represented by q_1 , and the geographical distance from node 2 to the grid point is represented by q_2 , the average frequency of the new grid node at time S+1 is:

$$\overline{\delta} = (q_2 l_{1,s+1} + q_1 l_{2,s+1}) / (q_2 l_{1,s} + q_1 l_{2,s})$$
 (3)

The average direction angle of these points can be obtained by the following formula:

$$\begin{split} l_{u,a} &= \int V_u(\delta, \phi) COS(\phi) f \delta f \phi \\ l_{u,b} &= \int V_u(\delta, \phi) SIN(\phi) f \delta f \phi \end{split} \tag{4}$$

The average direction angle of node u at time S can be obtained by the following formula:

$$\overline{\phi}_{u} = xTAN \left(\frac{l_{u,b}}{l_{u,a}} \right)$$
 (5)

The average direction angle of the sought point can be obtained by the following formula:

$$\overline{\phi} = xTAN \left(\frac{q_2 l_{1,b} + q_1 l_{2,b}}{q_2 l_{1,a} + q_1 l_{2,a}} \right)$$
 (6)

Based on the calculations of the node's average frequency and average direction angle, the spectral density of the sought point can be further determined:

$$V(\delta, \varphi) = q_2 V_1 \left[\overline{\delta}_1 \delta / \overline{\delta}, \varphi - (\overline{\varphi} - \overline{\varphi}_1) \right]$$

$$+ q_1 V_2 \left[\overline{\delta}_2 \delta / \overline{\delta}, \varphi - (\overline{\varphi} - \overline{\varphi}_2) \right]$$
(7)

Next, spectral density interpolation is performed using these data. The goal of spectral interpolation is to accurately map the spectral density matrix at time step S to the new grid nodes at time step S+1 through topological relationships. Since the grids at time steps S and S+1 may be different, traditional interpolation methods may not be directly applicable. Therefore, this paper adopts a distance-weighted interpolation method, combining the geographical position relationships and spectral density characteristics of the grid nodes before and after to perform the interpolation process. The interpolated spectral density matrix not only effectively updates the node information but also maintains the consistency and continuity of spectral energy in both frequency and direction.

The result of spectral density interpolation is a new two-

dimensional $V \times L$ matrix, where V represents the frequency segments and L represents the direction segments. This matrix provides accurate surface heat flow information for the new grid nodes at time step S+1. At this point, the surface heat flow field of the grid nodes at S+1 fully reflects the energy distribution from the previous time step while adapting to the new grid's geographical location and structural characteristics. Therefore, spectral density interpolation not only solves the information transfer issue caused by grid updates but also provides reliable heat flow data for subsequent temperature response predictions.

Real-time monitoring of rock temperature response requires efficient and accurate data processing methods. Considering that the rock mountain area is a large model area, the generated grid files contain a large number of node data, and traditional numerical methods may face problems such as large computational load and low computational efficiency when handling large-scale data. In order to achieve real-time monitoring of rock temperature responses, this paper chose to interpolate the spectral energy density matrices between the two grids, which can accurately transmit the heat flow field information from the previous time step to the next time step while ensuring efficiency. The interpolation method utilizes the relationship between the grids at the previous and next time steps to effectively estimate the spectral density distribution of the new grid nodes, avoiding data inconsistency caused by grid changes.

In order to achieve real-time monitoring of rock temperature response, three main interpolation methods were considered in this paper. The nearest point assignment method directly assigns the heat flow information of the new grid node to the heat flow data of the nearest old grid node. This method is simple, requires little computation, and can quickly obtain surface heat flow information for new nodes, making it suitable for scenarios where high computational speed is required. However, the nearest point assignment method is too simple and does not fully consider the spatial relationship between the new node and multiple nodes, so it may lead to large interpolation errors, especially in areas with complex geological structures or drastic heat flow changes. The linear interpolation method uses inverse distance weighting, where nearby nodes have a greater influence on the interpolation result. Specifically, using inverse distance weighting, nearby nodes have a larger effect on the result, thus more accurately reflecting local heat flow changes. To improve computational efficiency, this paper adopts a linear interpolation strategy based on the "window method." In this method, when the program is initially compiled, it filters all nodes and eliminates those far from the interpolation node, retaining only the nearby nodes for interpolation calculations.

The triangular area method is a geometry-based interpolation method, particularly suitable for handling grid nodes that are triangular elements. This method not only considers spatial topological relationships but also accurately reflects local variations of triangular grids. This method is suitable when there are significant changes in grid topology, especially in cases where high precision is needed to describe the heat flow distribution of new nodes, thus effectively improving the accuracy of interpolation results. Specifically, assume the energy density of the new node is represented by V_j , and the energy densities of the existing unit nodes X_j , Y_j are represented by V_j , V_j , V_j , V_j , and the areas of the triangular elements are V_j , V_j , V_j . The surface heat flow information for the newly inserted node can be obtained as follows:

$$V_i = V_x T_x + V_y T_y + V_z T_z \tag{8}$$

To achieve accurate rock temperature response prediction, this paper first uses the inverse distance weighted average method for surface heat flow information topology. This method can effectively capture local variations in the heat flow field while maintaining high computational efficiency. By introducing the "window method" in the interpolation process, nodes close to the new node are selected for weighted averaging, reducing computational load and thus improving computational speed. To further improve the model's operational efficiency, this paper introduces parallel computing technology, using multi-threading to process grid node information. In this way, although single-threaded computation may take longer, parallel computing can control topology time within 2 minutes, greatly improving overall computational efficiency.

Based on the above efficient computational methods, once accurate surface heat flow information is obtained in real time, it can be input into the temperature response model, and temperature changes at each node can be calculated through numerical simulation and physical equations. Specifically, using the heat conduction equation and considering boundary and initial conditions, the evolution process of the internal temperature of the rock with time and space can be simulated. In this process, the generation, propagation, and dissipation of heat flow are accurately considered and reflected, ensuring the accuracy of the simulation results. By continuously updating surface heat flow information and performing real-time temperature response calculations, this paper can dynamically monitor and predict temperature changes in rocks, promptly capturing the impact of geological events or structural activities on the temperature field, thereby achieving precise prediction of rock temperature response.

3. ROCK MOUNTAIN GEOLOGICAL STRUCTURE EVOLUTION SIMULATION BASED ON HEAT SOURCE TEMPERATURE INVERSION

In geological structure simulation, surface temperature is a key variable that directly affects the heat flow conduction, energy exchange, and geological processes of rock layers. The temperature of the rock surface is influenced by various factors, including solar radiation, long-wave radiation from the sky, sensible heat exchange, and latent heat exchange. These factors interact to cause the accumulation and dissipation of thermal energy at the rock surface. To achieve the simulation of the rock mountain geological structure evolution, this paper chooses to construct a surface energy heat balance equation. By constructing the surface energy heat balance equation, it is possible to comprehensively consider these heat exchange processes, thereby dynamically monitoring and estimating the temperature variation at the rock surface at different times and spatial scales. Specifically, assuming that solar shortwave irradiance and atmospheric longwave radiation are represented by R_{TY} and R_{TK} , the average shortwave absorption rate of the rock mountain surface is represented by β_1 , the average longwave emissivity of the rock mountain surface is represented by β_t , the surface radiation of the rock is represented by L_h , the sensible heat flux exchanged between the rock surface and the atmosphere is represented by G, the latent heat exchange flux is represented by RM, and the heat

conduction flux received by the rock surface is represented by H, the heat balance equation is expressed as:

$$\beta_1 R_{TY} + \beta_t R_{TK} - L_h + G + RM + H = 0$$
 (9)

In the construction of the rock mountain surface energy heat balance equation, six influencing factors each play different roles in the transmission and distribution of surface energy. To simulate the rock mountain geological structure evolution, these influencing factors must be accurately calculated and linked to the rock mountain surface temperature.

Solar shortwave irradiance is one of the main sources of energy input to the rock mountain surface and directly reflects the energy of solar radiation reaching the surface. When calculating solar shortwave irradiance, it is necessary to consider the influence of time, geographic location, seasonal variation, and other factors. These influences determine the intensity and distribution of solar radiation. Specifically, by considering the change in the solar angle, aerosol concentration in the air, and cloud cover, the radiation intensity received at the surface can be obtained. Since solar radiation directly impacts the surface temperature, this data is usually calculated through a radiation transmission model and corrected with meteorological data. Specifically, assuming the solar constant is represented by R_0 , atmospheric transparency is represented by O_l , the atmospheric mass number is represented by l, the cloud cover of the sky is represented by ZZD, and the solar zenith angle is represented by ϕ , the direct solar radiation received by the rock mountain surface R_{tf} can be calculated as:

$$R_{tf} = R_0 \cdot O_t^l \cdot ZZD \cdot COS\phi \tag{10}$$

Solar scattering can be calculated as:

$$R_{tt} = 0.5 \cdot R_0 \cdot \frac{\left(1 - O_t^l\right)}{1 - 1.4 \cdot LN(O_l)} \cdot ZZD \cdot COS\phi \tag{11}$$

The atmospheric mass number l is the relative optical mass of the atmosphere. Assuming that the atmosphere is a uniform medium, it can be considered that $l=1/SIN\psi$, where ψ is the solar altitude angle. Atmospheric transparency O_l refers to the ratio of the light intensity that passes through the atmosphere to reach the rock mountain surface to the incident light intensity. The relationship between the atmospheric transparency of one atmospheric mass O_l and the atmospheric transparency O_l at l atmospheric masses is as follows:

$$O_l = O_l^l \tag{12}$$

The cloud cover ZZD is:

$$ZZD = \left(1 - \frac{Z}{10}\right) \times 100\% \tag{13}$$

Atmospheric longwave radiation is determined by the temperature, humidity, and the presence of clouds in the atmosphere, reflecting the heat feedback from the atmosphere to the surface. Atmospheric longwave radiation is indirectly related to surface temperature and usually depends on the radiative characteristics of the atmosphere and environmental

conditions. When calculating this radiation, it is first necessary to consider variables such as the atmospheric temperature, humidity, and the optical thickness of the clouds, which together determine the intensity of atmospheric longwave radiation. The changes in atmospheric temperature and humidity directly affect the intensity of the radiation. Therefore, the calculation of atmospheric longwave radiation needs to be carried out through a radiation transmission model, using the temperature distribution of the atmosphere and water vapor concentration to deduce the transmission process of longwave radiation. Assuming the Stefan-Boltzmann constant is δ , the sky equivalent temperature is represented by S_{KQ} , and the actual water vapor pressure is represented by r_x , the formula for calculating atmospheric longwave radiation is:

$$R_{TK} = \delta \cdot S_{TK}^4 = \delta \cdot S_{KO}^4 \cdot (0.51 + 0.208\sqrt{r_x})$$
 (14)

The radiation of the rock mountain surface is the thermal radiation spontaneously emitted by the surface due to its temperature. When calculating this radiation, it is necessary to consider the variation in surface temperature and the emissivity of the surface material. The radiative intensity has a direct relationship with surface temperature, meaning that the higher the surface temperature of the rock, the stronger its radiative energy. Although the emissivity of rocks varies, typically, the surface will be adjusted according to the characteristics of its material. To accurately calculate this radiative flux, the Stefan-Boltzmann law is usually applied, and the radiative intensity is estimated based on the surface temperature and material properties. Assuming the surface temperature of the rock mountain is represented by S_t and the emissivity of the rock mountain surface is represented by γ , the formula for calculating the rock mountain surface's own radiation is:

$$L_h = \gamma \delta S_t^4 \tag{15}$$

The sensible heat flux is the heat released by the rock mountain surface through convection and conduction, directly influenced by the temperature difference between the surface and the air. The calculation of sensible heat flux depends on factors such as the temperature difference between the surface and the air, wind speed, and air density. When the wind speed is higher, heat from the air is more easily carried away, thus increasing the sensible heat flux. Sensible heat exchange is crucial for the dynamic regulation of surface temperature, especially in cases of significant weather changes, as it can significantly alter the surface heat distribution. Typically, the calculation of sensible heat flux requires considering meteorological data, temperature gradients, and the effect of air movement, using empirical models or numerical simulations to estimate it. Assuming the air density is represented by θ_x , the specific heat at constant pressure of the air is represented by Z_o , the drag coefficient is represented by Z_F , the wind speed is represented by i_x , and the atmospheric temperature at the reference height is represented by S_{gx} , the surface temperature of the rock mountain is represented by S_t , the sensible heat flux calculation formula is:

$$G = \mathcal{G}_x \cdot Z_o \cdot Z_F \cdot i_x \cdot \left(S_{gx} - S_t\right) \tag{16}$$

Latent heat exchange flux is mainly related to the evaporation or condensation process of surface moisture, reflecting the heat exchange between water vapor and air. The calculation of latent heat exchange first requires measuring changes in surface moisture, wind speed, air temperature, humidity, and other environmental parameters. These factors determine the rate at which water vapor transfers from the surface to the air and the amount of heat needed for the condensation or evaporation process of the moisture. Latent heat flux does not directly depend on the surface temperature of the rock mountain, but it indirectly affects the surface energy balance by influencing moisture transfer and variations in meteorological conditions. To calculate latent heat flux, empirical formulas or numerical simulation models based on meteorological factors such as wind speed, humidity, and temperature are typically used. Assuming the air density is represented by θ_x , the atmospheric specific humidity is represented by w_x , the surface specific humidity is represented by w_h , the latent heat of vaporization is represented by M, and the aerodynamic impedance is represented by E_x , the latent heat exchange flux calculation formula is:

$$RM = \mathcal{S}_x \cdot M \cdot \frac{w_x - w_h}{E_x} \tag{17}$$

Heat conduction flux describes the energy transferred downward from the rock mountain surface through heat conduction, and it is closely related to the thermal conductivity of the rock and the temperature gradient. When calculating this flux, it is first necessary to understand the thermal conductivity properties of different rock materials and determine the temperature gradient by measuring the temperature difference at the surface and at different depths. The larger the temperature gradient, the faster the heat transfer, so heat conduction flux has a direct relationship with surface temperature. The calculation of heat conduction usually relies on the thermal conductivity of the rock and temperature variations, using numerical simulation methods to estimate how heat is transferred within the rock. Assuming the thermal conductivity is represented by ε , and the thin layer depth used in the heat conduction flux calculation is represented by c, the heat conduction problem from the surface to the inner layer of the rock mountain is treated as a one-dimensional heat conduction problem:

$$H = -\varepsilon \frac{\partial S}{\partial c} \tag{18}$$

Assuming the surface temperature of the rock mountain is represented by S_t , the temperature at depth f is represented by S_{CON} , and the depth of the rock layer where the temperature remains constant is represented by f. Treating the problem in this paper as a steady-state heat conduction issue, the above equation can be written as:

$$H = \varepsilon \frac{S_{CON} - S_t}{f} \tag{19}$$

When there is a heat source inside the rock mountain, the heat inside the rock will gradually migrate upward, creating a certain temperature difference on the surface. At this time, the surface temperature S_{HE} , due to the heating effect of the internal heat source, will be significantly higher than the temperature S_{NON} , which is influenced only by external radiation heating. In this case, the internal heat source of the rock mountain mainly transfers heat to different depths of the rock layers through heat conduction, accumulating heat on the surface. During this energy transfer process, the surface temperature and the boundary layer temperature are influenced by multiple factors such as the intensity of the heat source, the thermal conductivity of the rock, and surface radiation. Figure 2 shows the three-dimensional spatial diagram of the internal temperature strategy of the rock mountain used in this paper. Figure 3 shows the isothermal surface diagram of the point heat source of the rock mountain.

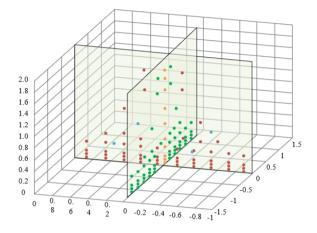


Figure 2. The three-dimensional spatial diagram of the internal temperature strategy of the rock mountain used in this paper

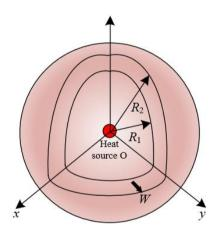


Figure 3. Schematic diagram of isothermal surfaces of the point heat source of the rock mountain

When there is no internal heat source in the rock mountain, the surface temperature is close to the average value of the daily air temperature, while the boundary layer temperature can be obtained through actual measurements. By combining these measurement data with the surface temperature S_{HE} under the condition of an internal heat source, the boundary layer temperature S_f at a specific depth f can be inferred, providing a basis for further estimating the intensity and distribution of the heat source.

$$\gamma \delta \left(S_{HE}^4 - S_{NON}^4 \right) = \frac{\varepsilon}{f} \left(S_{HE} - S_{NON} + S_u - S_f \right)$$
 (20)

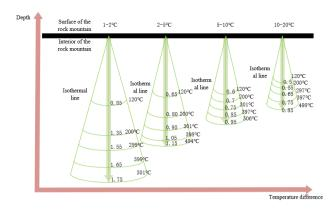


Figure 4. Example of the relationship between surface and deep temperatures of the rock mountain

The relationship between the surface and deep temperatures of the rock mountain is reflected in the fact that as depth increases, the temperature gradually rises, but the temperature increase slows down as the depth increases. An example is shown in Figure 4. This temperature-depth relationship typically follows an exponential distribution, meaning the temperature increases at a gradually slower rate with increasing depth. This pattern indicates that the heat conduction in the deep layers of the rock mountain mainly depends on the combined effect of the surface temperature and internal heat source, while also being influenced by the thermal conductivity and thermal diffusivity of the rock. Assuming the depth of the surface layer inside the rock mountain, unaffected by the external environment, is represented by f, and the temperature of the upper boundary layer at the depth f from the surface is represented by S_f , the relationship between temperature and depth is:

$$S = S_f \cdot y \cdot r^{x \cdot (E - f)} + z \tag{21}$$

Let the temperature growth coefficient be represented by x, and x and S_f are related following a Gaussian distribution, then:

$$x = 3.709 \cdot e^{-\left(\frac{S_f - 21.14}{6.778}\right)^2}$$
 (22)

Let the constant be represented by z, the depth of the heat source point from the surface of the rock mountain be represented by E, and the heat source temperature be represented by S. Let y and S_f be related following a quadratic distribution, then the relationship is:

$$y = d(S_f) = 0.008046S_f^2 - 0.3304S_f + 3.41$$
 (23)

The steps for simulating the geological structural evolution based on the inversion results of the heat source temperature can be further constructed by using the heat source depth and the upper boundary layer temperature obtained from the inversion. First, the proposed heat source depth inversion model is used to determine the depth of the heat source in the rock mountain, which is the first step of the simulation. By analyzing temperature data at different depths of the rock mountain, the heat source depth can be accurately inferred. Next, using the surface energy heat balance equation, combined with the known surface temperature and boundary layer temperature, the upper boundary layer temperature can

be inverted. Finally, combining the exponential growth relationship function of temperature and depth under "steady-state conduction," the heat source temperature is inverted using the heat source depth and upper boundary layer temperature obtained from the inversion as known values.

In the above process, by combining the temperature field distribution pattern with the characteristics of the heat source, the temperature distribution of the heat source at different depths can be obtained. Based on these temperature inversion results, the thermal evolution model of the rock mountain can be further constructed to simulate the evolution of the rock mountain under different heat sources and structural conditions. This model not only reveals the temperature changes of the rock mountain over a long time scale but also provides important input data for the dynamic process of geological structural evolution, promoting in-depth research into numerical simulations and evolutionary processes of the rock mountain's geological structure.

4. EXPERIMENTAL RESULTS AND ANALYSIS

From Figure 5, it can be observed that the average temperature in the rock model changes with axial strain in a certain regularity under different thermal expansion coefficients. As the axial strain increases, the temperature of the rock gradually rises, especially in the high-strain zone (such as when the strain exceeds 0.02), where the temperature increase becomes more significant. For example, when the axial strain is 0, the average temperature of the rock is 0, and as the strain gradually increases, the temperature also shows a gradual rise. Under different thermal expansion coefficients, the temperature response of the rock exhibits different rates and amplitudes of change, especially at the thermal expansion coefficients of 0.0455×10⁻⁶ and 0.0551×10⁻⁵, where the amplitude of temperature change with strain is relatively large. This change can be attributed to the influence of the thermal expansion coefficient on the accumulation and conduction of heat inside the rock. The larger the thermal expansion coefficient, the more significant the increase in internal temperature under strain. Furthermore, as axial strain increases, the rise in temperature also reflects the stress and thermodynamic changes the rock undergoes during the geological structure evolution process, especially when the strain reaches a critical value, after which the temperature rise becomes more gradual, indicating that the rock structure begins to stabilize.

From Figure 6, it can be observed that the range of the rock model changes with axial strain under different thermal expansion coefficients shows an obvious trend. Under low thermal expansion coefficients, as the axial strain increases, the range gradually increases from 0, and the increase is relatively smooth, reaching a maximum of 0.45. This indicates that under low thermal expansion conditions, the temperature response of the rock is more moderate, and the temperature change is less sensitive to strain. In contrast, under higher thermal expansion coefficients, as axial strain increases, the range rises significantly, especially when the strain exceeds 0.6, the range quickly jumps to 1.6, and continues to increase at a high rate as strain continues to increase. This indicates that a larger thermal expansion coefficient causes a greater temperature change in the rock under strain, and the thermal response of the rock becomes more sensitive, showing more significant changes in temperature range. The rock models with different thermal expansion coefficients exhibit a strong nonlinear relationship between temperature range and axial strain, especially in the larger strain range, where the temperature response is more pronounced.

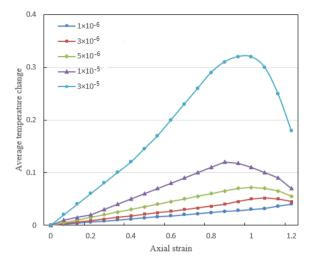


Figure 5. Change of average temperature with axial strain in the rock model under different thermal expansion coefficients

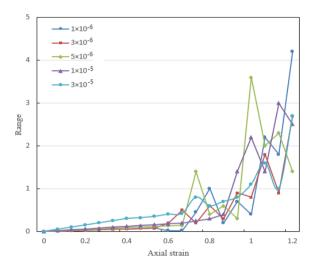


Figure 6. Change of range with axial strain in the rock model under different thermal expansion coefficients

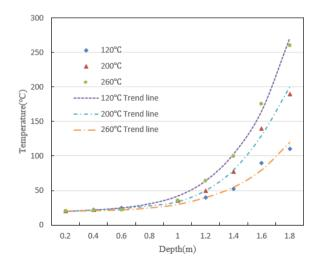


Figure 7. Temperature and depth relationship curve of the rock mountain under steady-state heat conduction

Based on the data provided in Figure 7 for the temperature and depth relationship curve under steady-state heat conduction conditions, it can be clearly observed that with the increase in depth, the temperature of the rock gradually increases. This trend has been verified under different temperature settings. Specifically, under the condition of 120°C, the temperature of the rock increases from 20°C to 270°C with increasing depth, and the temperature gradient remains relatively steady, with the largest change occurring in the depth range of 1.6 meters to 1.8 meters, showing a strong correlation between depth and temperature. Under conditions of 200°C and 260°C, the temperature of the rock exhibits a more obvious warming trend, especially at deeper depths (such as 1.4 meters and above), where the temperature change is more pronounced, indicating that the intensity and depth of the heat source have an important impact on the temperature distribution. From the trendline data, it can be seen that the rock temperature increases more significantly under higher temperature settings, and at deeper depths, the temperature rise is more substantial, particularly when the heat source temperature is high, leading to a significant increase in the temperature gradient.

Based on the above experimental data and the relationship between temperature and depth, it can be inferred that there may be regions in the geological structure where the heat source is more concentrated, especially in the depth range of 1.2 meters to 1.6 meters, where temperature changes are more dramatic. This may indicate uneven distribution of local heat sources, leading to a significant nonlinear change in the temperature field. This phenomenon is consistent with the geological occurrence of uneven heat source distribution and the accumulation of heat at depth. Furthermore, the change in temperature gradient suggests that the structural evolution of the region may include compression, folding, or faulting activities in the rock layers, which can influence the distribution of heat and its heating effect on the rock, further promoting changes in the temperature gradient.

 Table 1. Rock mountain upper boundary layer inversion experiment results

Heat Source Intensity	Surface Temperature of Active Temperature Field	Passive Temperature at the Boundary Layer	Active Temperature at the Upper Boundary Layer
115	25.6	16.5	18.9
216	28	16.5	22.65
257	28.4	16.5	21.5

According to the inversion experiment results of the upper boundary layer of Rock Mountain provided in Table 1, the temperature variation trends at the boundary layer under active and passive temperature fields can be observed. Specifically, when the heat source intensities are 115, 216, and 257, there are certain changes in the surface temperature and upper boundary layer temperature under the active temperature field. When the heat source intensity is 115, the surface temperature is 25.6°C, the passive boundary layer temperature is 16.5°C, and the active upper boundary layer temperature is 18.9°C. As the heat source intensity increases to 216, the surface temperature rises to 28°C, and the boundary layer temperature and upper boundary layer temperature are 16.5°C and 22.6°C, respectively. When the heat source intensity reaches 257, the surface temperature slightly increases to 28.4°C, while the

boundary layer temperature remains at 16.5°C, and the active upper boundary layer temperature is 21.5°C. These data show that with the increase of the heat source intensity, the surface temperature and upper boundary layer temperature in the active temperature field gradually increase, while the passive boundary layer temperature remains relatively constant, showing a clear influence of the heat source on the upper boundary layer. From the experimental results, it can be concluded that the heat source intensity significantly impacts the temperature field of the Rock Mountain boundary layer. As the heat source intensity increases, the surface and upper boundary layer temperatures gradually increase, especially in the active temperature field, where the temperature variation is more obvious. This indicates that the heat source intensity is directly positively correlated with the rock temperature variation. The stability of the passive boundary layer temperature might suggest a relatively stable geological structure background, where the heat source does not directly affect the deep rock structure or the heat conduction process is somewhat suppressed.

Table 2. Rock mountain heat source temperature inversion experiment results

Original Heat Source Intensity	Inferred Heat Source Temperature	Error Value	Relative Error
115	124.23	0.82	0.67%
216	213.26	1.56	0.81%
257	256.89	6.48	2.56%

According to the Rock Mountain heat source temperature inversion experiment results provided in Table 2, the matching of the original heat source intensity and the inferred heat source temperature can be observed. For a heat source intensity of 115, the original value is 115, the inferred value is 124.23, with an error of 0.82, and the relative error is only 0.67%. When the heat source intensity is 216, the original value is 216, the inferred value is 213.26, the error is 1.56, and the relative error is 0.81%. For a heat source intensity of 257, the original value is 257, the inferred value is 256.89, the error is 6.48, and the relative error is 2.56%. From these results, it can be seen that the heat source temperature inversion model can accurately invert the heat source temperature in most cases, especially under lower heat source intensities, where the relative error is small. As the heat source intensity increases, the relative error of the inversion result slightly increases, particularly for higher heat source intensities (257), where the error increases, but it remains within a reasonable range.

From the heat source temperature inversion experiment results, it can be seen that the model demonstrates high inversion accuracy under most heat source intensities. When the relative error is small, the inversion method is accurate and can restore the actual heat source temperature well, indicating that the heat source inversion method has high reliability in predicting temperature fields. However, at higher heat source intensities, the relative error increases, possibly due to the non-uniformity of the heat source at higher temperature gradients and the limitations of the model's calculations in high-temperature regions. This result suggests that, for larger heat source intensities, there may be more complex geological structures or heat source distributions, which require further optimization of the model's adaptability.

Based on the heat source temperature inversion error data provided in Figure 8, the variation trend between the inferred values and the true values can be observed. In the heat source temperature range from 120°C to 263.5°C, the inferred values are very close to the true values, and the difference between them is very small. Specifically, at different heat source temperatures, the difference between the inferred values and true values is relatively small, and the error value gradually increases, but remains within 1°C. For example, when the true value is 120°C, the inferred value is 120°C, with an error of 0°C; when the temperature increases to 140.5°C, the inferred value is 141°C, with an error of 0.5°C; at the maximum value of 263.5°C, the inferred value is 267°C, with an error of 3.5°C. Overall, the inversion error increases slightly with the temperature, but these errors are relatively small, indicating that the heat source temperature inversion method can predict the heat source temperature well in most cases.

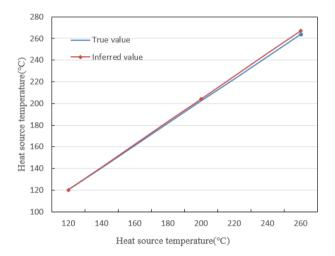


Figure 8. Heat source temperature inversion error chart

5. CONCLUSION

This paper proposed a new method based on thermodynamic theory for simulating rock temperature response and geological structure evolution, successfully achieving efficient and accurate prediction of temperature field distribution under complex geological structures and uneven heat source conditions. The research mainly includes two aspects: first, the use of the moving grid method to predict the rock temperature response, demonstrating the superiority of this method in handling complex geological environments; second, through the inversion of heat source temperature, the geological structure evolution of Rock Mountain is simulated, providing a more accurate basis for temperature field prediction. The experimental results show clear temperature distribution patterns at different heat source intensities, with small errors between the inferred values and true values, especially under low heat source intensities, where the inversion results show high accuracy and reliability. However, as the heat source intensity increases, the error slightly increases, but remains within an acceptable range. From this data analysis, it can be confirmed that the method proposed in this paper has significant effectiveness and potential in simulating rock temperature response and geological structure evolution.

The research in this paper provides a new perspective and method for thermodynamic analysis of geological structure evolution, especially in complex geological structures and uneven heat source conditions, enabling high-precision temperature field prediction. It has important scientific value and application prospects. The research results validate the effectiveness of the moving grid method and heat source temperature inversion method, laying a foundation for further in-depth research and practical applications. However, some limitations are also exposed in the research, such as the increase in temperature inversion errors under high heat source intensity conditions, reflecting the complexity and non-linear characteristics of the current method in handling hightemperature conditions. Further optimization improvement are still required. Future research directions can focus on the following aspects: first, further optimization of the inversion algorithm to improve accuracy under high heat source intensity conditions; second, increasing the diversity of data samples and experimental conditions to verify the broad applicability of the method; third, combining actual geological engineering cases to conduct larger-scale simulation experiments to verify the feasibility and reliability of the model in practical applications. Through continuous optimization and practical application, it is expected that this method will play a greater role in geological structure evolution research, providing scientific support for geological disaster warning and resource exploration.

ACKNOWLEDGMENT

This work was funded by the Science and Technology Development Program of Jilin Province, China (Grant No.: YDZJ202401525ZYTS).

REFERENCES

- [1] Yu, Z., Shao, J., Sun, Y., Wang, M., Vu, M.N., Plua, C. (2023). Numerical analysis of hydro-thermal fracturing in saturated rocks by considering material anisotropy and micro-structural heterogeneity. International Journal of Rock Mechanics and Mining Sciences, 170: 105457. https://doi.org/10.1016/j.ijrmms.2023.105457
- [2] Kumar, B., Bajpai, R.K., Singh, T.N. (2024). Comparative studies on heat and stress build up in jointed and intact granites at depth of 220 m, Bhima Basin, India. Current Science (00113891), 127(11): 1322-1329. https://doi.org/10.18520/cs/v127/i11/1322-1329
- [3] Guillemot, A., Audin, L., Larose, É., Baillet, L., Gueguen, P., Jaillet, S., Delannoy, J.J. (2024). A comprehensive seismic monitoring of the pillar threatening the world cultural heritage site Chauvet Pont d'Arc cave, toward rock damage assessment. Earth and Space Science, 11(4): e2023EA003329. https://doi.org/10.1029/2023EA003329
- [4] Ge, Y.K., Dai, J. G., Wang, C. S., Li, Y. L., Xu, G.Q., Danisik, M. (2017). Cenozoic thermo-tectonic evolution of the Gangdese batholith constrained by lowtemperature thermochronology. Gondwana Research, 41: 451-462. https://doi.org/10.1016/j.gr.2016.05.006
- [5] Liu, J.F., Luo, X., Feng, G., Zhou, L.L., Yang, X.G., Lu, G.D. (2023). Creep characteristics of thermally-stressed Beishan granite under triaxial compression. International Journal of Rock Mechanics and Mining Sciences, 162: 105302. https://doi.org/10.1016/j.ijrmms.2022.105302
- [6] He, J.T., Chen, B.L., Wang, Y. (2021). Structural deformation in Kaladawan of North Altun orogenic belt,

- NW China: Constraints from magnetic and EBSD fabrics. Geological Journal, 56(6): 3081-3096. https://doi.org/10.1002/gj.4090
- [7] Milicich, S.D., Wilson, C.J.N., Bignall, G., Pezaro, B., Bardsley, C. (2013). Reconstructing the geological and structural history of an active geothermal field: A case study from New Zealand. Journal of Volcanology and Geothermal Research, 262: 7-24. https://doi.org/10.1016/j.jvolgeores.2013.06.004
- [8] Mormone, A., Tramelli, A., Di Vito, M.A., Piochi, M., Troise, C., De Natale, G. (2011). Secondary hydrothermal minerals in buried rocks at the Campi Flegrei caldera, Italy: A possible tool to understand the rock-physics and to assess the state of the volcanic system. Periodico di Mineralogia, 80(3): 385-406. https://doi.org/10.2451/2011PM0027
- [9] Giacosa, R., Zubia, M., Sánchez, M., Allard, J. (2010). Meso-Cenozoic tectonics of the southern Patagonian foreland: Structural evolution and implications for Au-Ag veins in the eastern Deseado Region (Santa Cruz, Argentina). Journal of South American Earth Sciences, 30(3-4): 134-150. https://doi.org/10.1016/j.jsames.2010.09.002
- [10] Sun, H., Li, J., Zhang, Y., Dong, S., Xin, Y., Yu, Y. (2018). Early Paleozoic tectonic reactivation of the Shaoxing-Jiangshan fault zone: Structural and geochronological constraints from the Chencai domain, South China. Journal of Structural Geology, 110: 116-130. https://doi.org/10.1016/j.jsg.2018.03.003
- [11] Chen, X., Liu, J., Qi, Y., Bao, X., Ling, C. (2022). Middle-lower crustal flow in response to the India-Eurasia collision: Structural evidence from the southern Chong Shan belt within the Sundaland block, southeastern Tibetan Plateau. Geological Society of America Bulletin, 134(11-12): 2909-2932. https://doi.org/10.1130/B36244.1
- [12] Tao, B., Guoqiang, W., Botao, H., Zengchan, D., Lei, G. (2022). Neoproterozoic A-type granites in northern Beishan Orogenic Belt: Early response of the Rodinia supercontinent break-up. Acta Petrologica Sinica, 38(10): 2988-3002. https://doi.org/10.18654/1000-0569/2022.10.06
- [13] Xiao, R. (2020). Geological and tectonic evolution characteristics of polymetallic metallogenic belt.

- Arabian Journal of Geosciences, 13(18): 902. https://doi.org/10.1007/s12517-020-05847-0
- [14] Meng, H., Mei, G., Qi, X., Xu, N., Peng, J. (2024). Deep generative model-based generation method of stochastic structural planes of rock masses in tunnels. Geological Journal, 59(9): 2566-2583. https://doi.org/10.1002/gj.5000
- [15] Yu, Y., Yang, Y., Liu, J., Wang, P., Liu, J., Song, Z., Zhao, S. (2023). Mechanical characteristics and energy evolution in a rock mass with a weak structural plane. Scientific Reports, 13(1): 18674. https://doi.org/10.1038/s41598-023-46180-2
- [16] Ren, Y.Y., Sun, Y.D., Meng, X.X. (2023). Multi-scale structural characteristics and the damage evolution mechanism of rock under load. Materials Letters, 331: 133430. https://doi.org/10.1016/j.matlet.2022.133430
- [17] De Vita, P., Carratù, M.T., La Barbera, G., Santoro, S. (2013). Kinematics and geological constraints of the slow-moving Pisciotta rock slide (southern Italy). Geomorphology, 201: 415-429. https://doi.org/10.1016/j.geomorph.2013.07.015
- [18] Quốc Cu'ò'ng, N., Tokarski, A.K., Świerczewska, A., Zuchiewicz, W.A., Yêm, N.T. (2013). Late Tertiary tectonics of the Red River Fault Zone: Structural evolution of sedimentary rocks. Journal of Geodynamics, 69: 31-53. https://doi.org/10.1016/j.jog.2012.05.002
- [19] Carpinteri, A., Lacidogna, G., Manuello, A., Borla, O. (2012). Piezonuclear fission reactions in rocks: Evidences from microchemical analysis, neutron emission, and geological transformation. Rock Mechanics and Rock Engineering, 45(4): 445-459. https://doi.org/10.1007/s00603-011-0217-7
- [20] Kozlov, N.E., Sorokhtin, N.O., Martynov, E.V. (2018). Geodynamic evolution and metallogeny of Archaean structural and compositional complexes in the northwestern Russian Arctic. Minerals, 8(12): 573. https://doi.org/10.3390/min8120573
- [21] Tian, F., Guo, T., He, D., Gu, Z., Meng, X., et al. (2024). Three-dimensional structural models, evolutions and petroleum geological significances of transtensional faults in the Ziyang area, central Sichuan Basin, SW China. Petroleum Exploration and Development, 51(3): 604-620. https://doi.org/10.1016/S1876-3804(24)60491-X